Journal of Physics: Conference Series **303** (2011) 012058 doi:10.1088/1742-6596/303/1/012058

Substrate-induced magnetic anisotropy in $La_{0.7}Sr_{0.3}MnO_3$ epitaxial thin films grown onto (110) and (1$\bar{1}$8) $SrTiO_3$ substrates

P Perna[1], C Rodrigo[1,2], E. Jiménez[1,2], N Mikuszeit[1,2], F J Teran[1], L Méchin[3], J Camarero[1,2] and R Miranda[1,2]

[1] Instituto Madrileño de Estudios Avanzados en Nanociencia, IMDEA-Nanociencia, Campus Universidad Autónoma de Madrid, 28049 Madrid, Spain
[2] Departamento de Fisica de la Materia Condensada and Instituto "Nicolás Cabrera", Universidad Autónoma de Madrid, 28049 Madrid, Spain
[3] GREYC (UMR6072) CNRS-ENSICAEN and Université de Caen Basse-Normandie, Bd. de Marèchal Juin, 14050 Caen, France

E-mail: paolo.perna@imdea.org

Abstract. We show a detailed magneto-optical Kerr study at room temperature of well characterized epitaxial $La_{0.7}Sr_{0.3}MnO_3$ (LSMO) thin films grown onto (110) and (1$\bar{1}$8) $SrTiO_3$ substrates. The films present a well-defined uniaxial (two-fold) magnetic anisotropy ascribed to substrate-induced anisotropy. In particular, the in-plane uniaxial anisotropy in the(110)-oriented LSMO films originates from the existence of elongated in-plane [001]-oriented structures. Similar elongated structures, parallel to the [110] crystallographic direction, are found for LSMO films grown on (1$\bar{1}$8) STO surfaces. In all films, such a uniaxial magnetic anisotropy is characterized by an easy axis lying along the elongated structures. Furthermore, the vectorial-resolved hysteresis loops as a function of the in-plane applied field direction are interpreted in terms of rotation and propagation and nucleation of magnetic domains processes. Our results demonstrate the tailoring of magnetic anisotropy by exploiting the substrate-induced anisotropy in epitaxial thin films.

1. Introduction

In epitaxial magnetic thin films the cubic crystal symmetry can be broken by atomic steps on the surface or by anisotropic lattice relaxation, inducing an additional in-plane uniaxial magnetic anisotropy contribution. Such a symmetry breaking has been demonstrated in epitaxial magnetic thin films with cubic symmetry in half metallic manganese-based oxides [1, 2], as well as in metal systems [3] and in diluted semiconductors [4]. The competition between the biaxial (four-fold) and the additional uniaxial (two-fold) anisotropy results in a magnetic reorientation, which depends on many parameters, such as substrate step density [3], thickness [1], angle of deposition [5], and even the temperature range [1]. Thus, the symmetry breaking in magnetic systems provides an additional contributions to the magnetic anisotropy, which could alter both magnetization easy and hard axis and reversal processes [6]. In order to control and tailor the magnetic properties of materials, it is possible to resort to the fabrication of artificial nanostructures [7], thin films [8, 9, 10] and superlattices [11].

In this work, we resort to the interesting properties of the magneto-resistive mixed-valence manganese oxides, $La_{0.7}Sr_{0.3}MnO_3$ (LSMO) that shows both a Curie temperature above 300 K and an almost 100% spin polarization. We have engineered the growth of epitaxial films in order to obtain purpose-designed magnetic anisotropy exploiting to anisotropy induced by substrates with different crystallographic orientation, which can be employed for the fabrication of spintronics devices, operating at room temperature (RT), such as read-heads magnetic hard disks and non-volatile magnetic memories [12]. In this system, the substrate can induce tensile or compressive strain to the film depending on the film-substrate lattice mismatch, determining in-plane or out-of-plane easy magnetization directions, respectively [13]. In particular, the strain in LSMO thin films deposited on $SrTiO_3$ (STO)(001) is in-plane tensile and an in-plane biaxial magnetic anisotropy is generally observed, with the easy in-plane direction along $\langle 110 \rangle$, and the hard in-plane direction along $\langle 100 \rangle$ [13, 14]. In the particular case of LSMO grown onto STO(110), the substrate induces a strain that is anisotropic in-plane, i.e. the two in-plane directions of strain are inequivalent. This causes an in-plane uniaxial magnetic anisotropy with the easy axis (e.a.) of magnetization along the [001] crystallographic direction [9]. Another possibility to induce in-plane magnetic anisotropy is to create artificially periodic stepped surfaces by exploiting vicinal substrates [2]. These substrates are intentionally misoriented to a (near) low index surface, therefore determining surface step edges. In such a way, the high symmetry of the low index surface is broken, and an additional uniaxial anisotropy is expected [15]. Matthews *et al.* have reported an in-plane uniaxial magnetic anisotropy at RT in 25 nm and 7 nm thick LSMO films deposited on very low miscut STO substrates (0.13° and 0.24°), which vanishes at low temperatures [1]. Uniaxial magnetic anisotropy with easy axis along the step edges has been found at 80 K for a 12.6 nm thick LSMO film deposited on a vicinal STO(001) substrate with a 10° miscut off the [001] plane toward the [010] crystallographic direction [16].

2. Structural and morphological characterizations

70 nm thick LSMO thin films were deposited by pulsed laser deposition (PLD) from a stoichiometric target onto commercially available STO(110) and vicinal STO($1\bar{1}8$) substrates. In the latter case the vicinal angle was 10° from the [001] surface towards the [$1\bar{1}0$] crystallographic direction, thus inducing step edges along the [110] direction [2]. The optimization of the growth conditions was performed on standard STO (001) substrates [11]. The laser fluence was $1-2$ J cm^{-2}, the target-to-substrate distance was 50 mm, the oxygen pressure was 0.35 mbar and the substrate temperature was 720 °C.

The crystal structure was investigated by means of X-ray Diffraction (XRD). Standard θ-2θ scans were routinely performed in order to determine the out-of-plane lattice parameters. The XRD $\theta - 2\theta$-scans indicate that the LSMO films were epitaxially grown on the substrates. In particular, the LSMO films grown onto STO(110) present the (110) axis coincident with the (110) axis of the substrate, as well as the LSMO film grown onto vicinal STO(001) presents the (001) axis parallel to the (001) axis of the substrate [2]. In the case of vicinal LSMO films, the offset angle was checked to be equal to the substrate vicinal angle within ±0.05°. The out-of-plane and the in-plane lattice parameters were determined by XRD measurements around symmetric and asymmetric crystallographic peaks. In the case of the LSMO/STO(110), the two inequivalent in-plane directions of strain induced by the STO are the [001] and [$1\bar{1}0$], which determine two different in-plane strain tensor componentes, $\epsilon_{[001]} = 0.80\%$ and $\epsilon_{[1\bar{1}0]} = 0.30\%$. The measured lattice parameters and the strain tensor component along the [100] ($\epsilon_{[100]}$) in-plane crystallographic direction for the LSMO grown onto vicinal (001)-oriented STO substrates present the two in-plane lattice parameters of the LSMO cell equally tensile strained ($\epsilon_{[100]} = \epsilon_{[010]} = 0.80\%$) by the substrate. The crystalline quality of the films was checked by measuring the Full-Width-Half-Maximum (FWHM) of the rocking curves (ω-scan), which are always found below 0.15°, and the in-plane crystal plane alignement (ϕ-scan).

The morphology of the samples were investigated at room temperature by means of atomic force (AFM) and scanning tunnel microscopies (STM), using a Nanoscope microscope [2]. The average roughness (RMS) of the samples was found always in the range of few unit cells (u.c.). In general, the morphology of the LSMO films replicates that of the substrates for all samples investigated. In the case of the LSMO/STO(110), the particular morphology of the substrate surface induces film structures elongated along the in-plane [001] crystallographic direction, corresponding to the direction of the higher in-plane tensile strain value (see inset in Fig. 1). LSMO films deposited onto 10° vicinal STO(001) substrate present similar elongated structures on the top surface oriented along the $[1\bar{1}0]$ crystallographic direction (see inset in Fig. 2).

A detailed characterization of the films is reported in Ref. [2]. It is worth noting that in all the investigated samples, the Curie temperature was always found above RT.

3. Magneto-optical Kerr characterization

The magnetic anisotropy of the films and the angular dependence of the magnetization reversal were investigated at RT by high-resolution vectorial-Kerr magnetometry measurements. In our setup the combination of p-polarized incident light in Kerr experiments and the simultaneous detection of the two orthogonal components of the reflected light allow the simultaneous determination of the components of the in-plane magnetization, parallel ($M_{\parallel}$) and perpendicular ($M_{\perp}$) to the magnetic field direction [17].

The samples were mounted in a stepper-motorized eucentric goniometer head that keeps the reflection plane fixed for the whole set of experiments. In magnetooptical measurements this is important to be able to compare the values of the magnetization components measured at different rotation angles and between different samples. The study of the magnetization reversal processes as well as magnetic anisotropy of the films was performed by measuring simultaneously the in-plane vectorial-resolved hysteresis loops, i.e., $M_{\parallel}(H,\theta)$ and $M_{\perp}(H,\theta)$, as a function of the sample in-plane angular rotation angle (θ), keeping fixed the external magnetic field direction. The whole angular range was probed every 4.5°, with 0.5° angular resolution.

3.1. LSMO grown onto STO(110)

Representative in-plane vectorial-resolved Kerr hysteresis loops of 70 nm thick LSMO film grown onto STO(110) acquired at selected angles θ are shown in Fig. 1. The angle $\theta = 0°$ is taken when the external field is aligned parallel to the [001] in-plane crystal direction, i.e. lying along the elongated structures visible on the film surface.

Both magnetization components, i.e., parallel ($M_{\parallel}$) and perpendicular ($M_{\perp}$) to the external magnetic field, show either sharp irreversible transitions and/or smoother fully reversible transitions, in dependence of θ. Taking into account the extended character of the film, the irreversible transitions correspond to nucleation and further propagation of magnetic domains and the reversible ones correspond to magnetization rotation processes [2]. For $\theta = 0°$ the parallel component presents a perfect squared shape hysteresis loop (central top graph of Fig. 1). $M_{\parallel}$ does not change from the saturation (M_S) to the remanence ($M_{\parallel,R}$), i.e., $M_{\parallel,R}/M_S \approx 1$, and there is only a sharp irreversible jump at the coercive field $\mu_0 H_C = 1.50$ mT, in which the magnetization reverses. In turn the perpendicular component is negligible in the whole field loop, i.e., $M_{\perp}(H) \approx 0$. Both are expected behaviors of a magnetization e.a. direction, in which the magnetization reversal takes place via nucleation and further propagation of magnetic domains oriented parallel to the field direction [2].

For $\theta \neq 0°$, clear $M_{\perp}(H)$ loops with both reversible and irreversible transitions are found, in correspondence to the $M_{\parallel}(H)$ loops, as shown by the left and right graphs of Fig. 1. In particular, for $\theta \pm 18°$ the irreversible switching field of the perpendicular component is $\mu_0 H_S(\pm 18°) = 1.55$ mT, identical to $\mu_0 H_C(\pm 18°)$. In addition, the $M_{\perp}(H)$ loops acquired at opposite angles present similar shape but different sign. The latter arises from the sensitivity

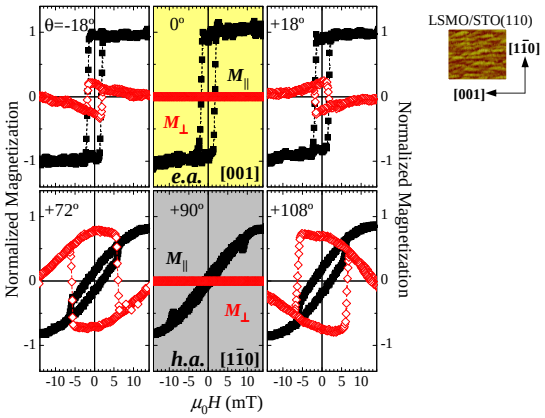

Figure 1. Magnetization reversal study of a 70 nm thick LSMO film grown onto a (110)-oriented STO substrate around the e.a. (left panel) and h.a. (right panel) directions. The corresponding applied field angles θ are indicated in the graphs. The experimental $M_\parallel(H)$ and $M_\perp(H)$ loops are given by filled black and open red circles, respectively. The inset shows the STM (300×300 nm^2) image of the LSMO surface.

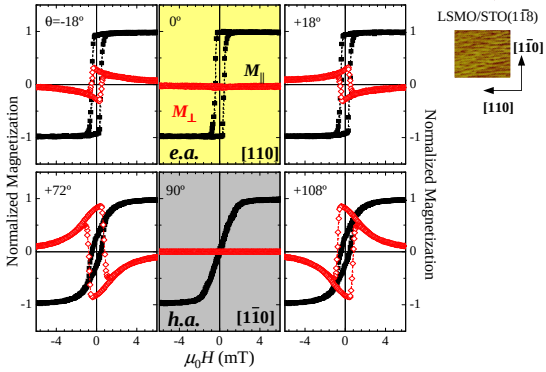

Figure 2. Magnetization reversal study of the 70 nm thick LSMO film grown onto vicinal 10° STO(001) substrate around the e.a. (left panel) and h.a. (right panel) directions. The corresponding applied field angles θ are indicated in the graphs. The experimental $M_\parallel(H)$ and $M_\perp(H)$ loops are given by filled black and open red symbols, respectively. The inset shows the STM (300×300 nm^2) image of the LSMO surface.

of $M_\perp(H)$ to the anisotropy direction [18]. Therefore, around the e.a. direction, the reversible transitions correspond to a reversal by magnetization rotation whereas the irreversible ones correspond to nucleation a propagation of magnetic domains not oriented parallel to the field direction but to the e.a. direction which, in the present case, is aligned parallel to the elongated structures.

3.2. LSMO grown onto STO(1$\bar{1}$8)

Well-defined uniaxial anisotropy is also found in LSMO/STO(1$\bar{1}$8) systems. Fig. 2 shows representative Kerr hysteresis loops of a 70 nm thick film grown onto vicinal STO(001) surface, with a 10° miscut off the [001] plane toward the [1$\bar{1}$0] crystallographic direction, at selected angles θ between the magnetic field and the surface steps direction. $\theta = 0°$ is hence taken when the external field is aligned parallel to the [110] in-plane crystal direction. As before, the characteristic axes are located precisely at the change of sign of the $M_\perp(H)$ loops. Hence, the e.a. direction is along the direction of the steps (i.e., [110]) and the h.a. is perpendicular to it (i.e., [1$\bar{1}$0]).

The evolution of the vectorial-resolved hysteresis loops is analogous to the flat LSMO(110) film. Hence, the relevant mechanism for the magnetization reversal close to the e.a. direction is the nucleation and propagation of magnetic domains oriented parallel to the elongated structures, i.e., parallel to the steps, whereas reversal by rotation processes are the relevant mechanism close to the h.a. direction, i.e., perpendicular to the steps. This picture has been strongly supported recently in real space by means of angular dependence Kerr microscopy measurements [19].

4. Summary

For both the investigated systems the angular dependence of the normalized remanence values of both magnetization components, i.e., $M_{\parallel,R}/M_S$ and $M_{\perp,R}/M_S$ shows a pronounced oscillation of both magnetization components with periodicity of 180°, the parallel component follows a $|\cos\theta|$ law, the perpendicular component changes the sign when a characteristic direction, i.e., e.a. and h.a. directions, is crossed (Fig. 3(a),(b)). The polar-plot of $M_{\parallel,R}/M_S$ shown in Fig. 3 shows the characteristic "two-lobe" behavior, originated from a two-fold symmetry. All these features confirm the uniaxial magnetic anisotropy behavior of the film, where the anisotropy axis is aligned parallel with the direction of the elongated grains, i.e. parallel to the in-plane [001] crystallographic direction. Both experimental hysteresis loops and remanence magnetization have been properly reproduced in the whole angular range with the Stoner-Wolfhart (SW) model depicted in Ref. [2, 6] (Fig. 3(a),(b)). In order to reproduce satisfactorily the experimental data, in such a simple coherent rotation SW model, only the uniaxial anisotropy term (K_u), arising from the two-fold film morphology, has been taken into account, neglecting completely the biaxial term (K_b), arising from the four-fold crystal symmetry.

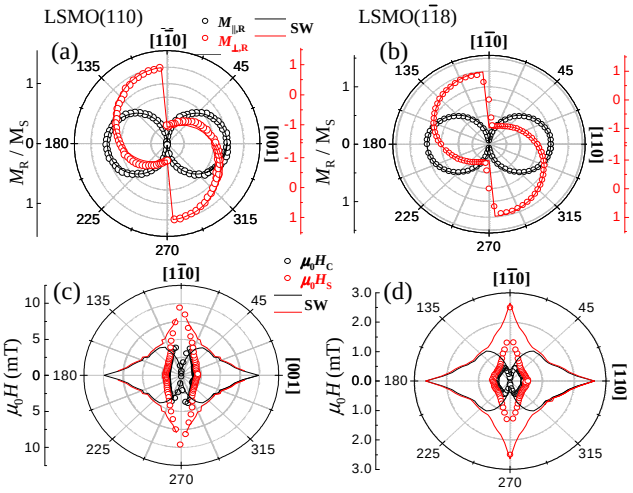

Figure 3. (Color online) Top graphs show the polar plot representations of the angular evolution of the in-plane normalized remanence of magnetization ($M_{\parallel,R}/M_S$ and $M_{\perp,R}/M_S$) of 70 nm thick LSMO films grown onto (a) STO(110) and (b) vicinal STO(001) substrates. Bottom graphs show polar plot representation of both coercive (H_C) and switching (H_S) fields of 70 nm thick LSMO films grown onto (c) STO(110) and (d) vicinal STO(001) substrates. The symbols are the corresponding experimental values obtained from the vectorial-resolved hysteresis loops. The continuous lines represent the expected behavior from the SW model described in the text, which only considers the uniaxial anisotropic term derived from the experimental data.

It is worth noting that such a theoretical model, which assumes a single particle behavior, takes into account only coherent magnetization reversal by switching (irreversible process) and/or rotation (reversible), where it fails where other irreversible magnetization reversal processes, like nucleation and propagation of magnetic domains, dominate. The latter can be energetically more favorable in systems in which defects—structural or morphological—play the main role to activate irreversible magnetic domain nucleation processes at magnetic fields that are significantly lower than expected by the SW model. This defects can act as pinning centers for the created magnetic domain walls and the reversal further continues via domain wall propagation. Hence, in our case, the simulated loops of both coercive (H_C) and switching (H_S) fields, extracted numerically by the SW model depicted in Ref. [2], overestimates the

coercive field near the e.a., where irreversible transitions for the magnetization reversal due to the presence of pinning centers dominate (Fig. 3(c),(d)). The angular evolution of the remanence magnetization (Fig. 3(a),(b)) as well as both coercive and switching fields (Fig. 3(c),(d)), presents 180° periodicity. The expected behavior from the numerical simulations are also superimposed to the experimental data in order to verify the good qualitative agreement of model and experiment. Again the rotation model reproduces satisfactorily both $M_{\parallel,R}$ and $M_{\perp,R}$ in the whole angular range whereas it fails to reproduce $\mu_0 H_C$ and $\mu_0 H_S$ close to e.a. directions. In contrary, close to the h.a. direction, where reversible processes are the relevant mechanism during reversal, the rotation model reproduces satisfactorily the coercive and switching fields behavior.

In conclusion, we have investigated the magnetic anisotropy of LSMO thin films by high-resolution vectorial Kerr magnetometry. The dominance of the uniaxial anisotropy over the biaxial anisotropy is achieved in LSMO thin films grown onto STO(110) and STO($1\bar{1}8$) susbtrates. In both systems, the surface-induced anisotropy determines a well defined uniaxial magnetic anisotropy, with the e.a. lying along the direction of surface step edges. We have also shown the angular dependence of the magnetization reversal processes from the detailed analysis of the vectorial-resolved Kerr loops. Nucleation and further propagation of magnetic domains and rotation processes are the relevant mechanism during magnetization reversal around the e.a. and h.a. directions, respectively. The angular dependence of both switching and coercive fields for θ near the e.a. and h.a. directions can be understood in the framework of the pinning and SW models, respectively. We demonstrated the ability to control and tailor the magnetic properties of LSMO thin films which is an important task for the design of novel devices based on thin film technology.

ACKNOWLEDGEMENTS

This work was supported in part by the Spanish MICINN through Project No. CSD2007-00010 and by the Comunidad de Madrid through Project No. S2009/MAT-1726. P.P. thanks the European Science Foundation (ESF) through the activity entitled 'Thin Films for Novel Oxide Devices' (http://www.ims.tnw.utwente.nl/thiox/) for partial financial support through exchange grants.

5. References

[1] M. Mathews, *et al.*, Appl. Phys. Lett. **87**, 242507 (2005).
[2] P. Perna, *et al.*, "Tailoring magnetic anisotropy in epitaxial half metallic $La_{0.7}Sr_{0.3}MnO_3$ thin films", *submitted to* (2010).
[3] A. Berger, *et al.*, Phys. Rev. Lett. **68**, 839 (1992).
[4] U. Welp, *et al.*, Phys. Rev. Lett. **90**, 167206 (2003).
[5] S. van Dijken, *et al.*, Phys. Rev. B **63**, 104431 (2001).
[6] D. Ecija,*et al.*, Phys. Rev. B **77**, 024426 (2008); *ibid.* J. Magn. Magn. Mater. **316**, 321 (2007).
[7] J. J. de Miguel and R. Miranda, J. Phys.: Condens. Matter **14**, R1063 (2002).
[8] M. Radovic, *et al.*, Appl. Phys. Lett. **94**, 022901 (2009)
[9] A. Ruotolo, *et al.*, Appl. Phys. Lett. **88**, 252504 (2006).
[10] A. Ruotolo, *et al.*, Appl. Phys. Lett. **91**, 132502 (2007).
[11] P. Perna, *et al.*, J. Phys.: Condens. Matter **21**, 306005 (2009).
[12] J.-H. Park, *et al.*, Nature **392**, 794 (1998).
[13] F. Tsui, *et al.*, Appl. Phys. Lett. **76**, 17 2421 (2000).
[14] M. Ziese, *et al.*, J. Mag. Mag. Mat. **246**, 327-334 (2002).
[15] R.A. Hyman, *et al.*, Phys. Rev. B **58**(14), 9276 (1998).
[16] Z.-H. Wang, *et al.*, Appl. Phys. Lett. **82**(21), 3731 (2003).
[17] J. Camarero, *et al.*, Phys. Rev. Lett. **95**, 057204 (2005).
[18] E. Jiménez, *et al.*, Phys. Rev. B **80**, 014415 (2009).
[19] P. Perna, *et al.*, "Imaging the magnetization reversal of step-induced uniaxial magnetic anisotropy in vicinal epitaxial $La_{0.7}Sr_{0.3}MnO_3$ films", *submitted to* (2010)